KRONOS FUSION ENERGY

PAPER 2.8 · THE KRONOS 2026 SERIES

Vertical Stability at High Elongation: Displacement Growth Rates, Control-Coil Authority, and VDE Avoidance for a Compact Spherical-Tokamak Breeder

Elongation buys confinement in a compact machine, and it is not optional: the Hyperion spherical-tokamak breeder holds at elongation with negative triangularity , aspect ratio and...

Read it live — 3-D model · physics validator · film series

BY P I FORD

2026 · EDITORIAL EDITION

THE OFFICIAL RECORD

What this document is, and how to read its numbers

This is a combined editorial. It gathers, in one volume, the two design studies Kronos Fusion Energy released in 2026 — a compact spherical-tokamak tritium/helium-3 breeder and a deuterium–helium-3 tandem-mirror generator — together with the intellectual-property estate, the people, and, in the internal edition, the full commercial case. The scientific text is the same text that appears in the arXiv preprints and the journal submissions; the editorial adds the apparatus a reader needs to hold the whole program at once, and nothing in the physics is altered to fit it.

THE HONESTY STANCE IS THE ASSET

Every headline quantity carries an **evidence class** — DERIVED RECOMPUTED MEASURED REQUIREMENT — and, where a number is a modelled extrapolation rather than a demonstrated value, it is labelled as such and its downside is shown next to it. Several quantities in the underlying corpus moved after first publication; where a value has been withdrawn or restated, the record says so plainly. This is deliberate: a diligence team will find the load-bearing assumptions, so the document surfaces them first.

TWO EDITIONS

This volume is issued in two editions. The **public edition** (light) carries the physics and the design only — no dollar, price, or per-kilogram figure appears anywhere in it. The **internal edition** (dark) adds the economics, the funding architecture, and the defense-commercial analysis, and is marked *Confidential* accordingly; it is not for public distribution. Where the commercial case rests on a modelled assumption rather than a demonstrated one, it is labelled as such and its downside is shown alongside it, on the same terms as the physics.

TITLE	The Kronos Fleet — Hyperion · Aegis · MetroVolt: A Combined Design & Commercialization Study
AUTHOR	Priyanca Ford, Founder & CEO, on behalf of Kronos Fusion Energy
EDITION	2026 Combined Editorial · first issue
COMPANION WORKS	The five-paper arXiv drop — (1) Breeder, (2) Burner, (3) REBCO magnet & tape, (4) Direct Energy Conversion, (5) AI/ML/Quantum control — with matching numbered Zenodo deposits, plus the IOP journal and IAEA-FEC submissions. Patents were filed before the drop.
NAMING	Hyperion = the breeder; Aegis (defense) and MetroVolt (data-center) = one generator in two housings. Internal mode letters (D1, L) do not appear on public surfaces.
STATUS	Conceptual design & simulation study. Nothing herein is a construction commitment.

HOW TO READ THIS VOLUME

The fleet at a glance, and the way its numbers are marked

This volume opens with *Orientation*, presents the five research papers as a bound sequence, and closes with the *Apparatus*. *Foundations* sets out the three general results both machines rest on. *Paper One* is the Hyperion breeder; *Paper Two* the Aegis / MetroVolt generator; *Papers Three, Four and Five* are the enabling science — high-field REBCO magnets and tape, direct energy conversion, and the AI / ML / quantum control stack. A *Digital Twin & 3-D Model* part follows, then the *Environmental* profile. The *Economics* and levelized cost and the *Business Case* and diligence record appear in the internal edition only; the *Simulations* proof record and the Apparatus — patent portfolio, team, limitations, and sources — close both editions.

THE FLEET AT A GLANCE

	HYPERION	AEGIS	METROVOLT
Role	Strategic-isotope foundry	Defense installation power	Campus power
Machine	**Spherical tokamak**	**Tandem mirror**	**Tandem mirror**
Fuel	Deuterium–tritium	Deuterium–helium-3	Deuterium–helium-3
Delivers	Tritium · ^{3}He · 14 MeV n	Resilient installation power	Firm campus power
Physics bar	**Fusion gain only**	Closure (gates named)	Closure + lunar ^{3}He
In the fleet	Breeds the fuel	Proves the generator	Commercial destination

HOW THE NUMBERS ARE MARKED

Every headline quantity carries an evidence class — DERIVED from first principles, RECOMPUTED from raw data, MEASURED in hardware, or a REQUIREMENT yet to be met. Financial figures carry a case label and are confined to the internal (confidential) edition. Values that moved after first publication are shown as withdrawn or restated rather than quietly changed. A capability you can evaluate is one whose limits are on the page.

ABSTRACT

Vertical Stability at High Elongation: Displacement Growth Rates, Control-Coil Authority, and VDE Avoidance for a Compact Spherical-Tokamak Breeder

Elongation buys confinement in a compact machine, and it is not optional: the Hyperion spherical-tokamak breeder holds $I_p = 9.66\,MA$ at elongation $\kappa = 2.0$ with negative triangularity $\delta = -0.30$, aspect ratio $A = 2.5$ and major radius $R_0 = 1.20\,m$. The price of that elongation is a passive axisymmetric vertical instability, and in a spherical tokamak the instability is fast. We pose the vertical-control problem formally, from the massless rigid-displacement force balance through the passive-vessel circuit to a proportional– derivative (PD) feedback loop closed on the poloidal-field (PF) coils, and we solve it on the canonical free-boundary equilibrium reconstructed by a GPU-accelerated Grad–Shafranov solver. A single mechanistic result organises the analysis: the normalised growth rate obeys $\gamma\tau_w = \hat{k}/(1-\hat{k})$, where $\hat{k}$ is the destabilising-to-wall coupling and $\hat{k} \to 1$ is the ideal wall limit. At $\kappa = 2.0$ the vessel vertical-mode wall time is $\tau_w = 11.9\,ms$ and $\gamma\tau_w = 8.05$, so $\hat{k} = 0.890$, $\gamma = 677\,/s$ and the growth time is $1.48\,ms$ — spherical-tokamak-typical (NSTX-class). A PD controller on the PF coils arrests the mode: a direct eigenvalue solve of the closed-loop system places a fast pole at $-964\,/s$ (faster than the open-loop growth) and a slow resistive-relaxation pole at $-14\,/s$; the stabilising proportional gain threshold is $K_p^* = 30302\,V/m$ and the damping threshold is $K_d^* \approx 1156$. From a 5 mm disturbance the excursion peaks at only 8.1 mm at $t \approx 3.54\,ms$ and reverses, requiring a PF converter of $\sim 49\,Mvoltampere$ (10.1 kV, 4.9 kA, 5.0 kA/ms). The elongation carries headroom: the feedback ceiling $\gamma\tau_w \approx 15$ is reached at $\kappa_{\max} \approx 2.37$, so the operating point sits 19% below the controllable limit, with the converter growing super-linearly ($49 \to 91\,Mvoltampere$) toward it. The worst case is bounded: a vertical displacement event terminating in a disruption gives a halo current of $\sim 2.9\,MA$ and a peak vertical force of $\sim 23\,MN$, a structural specification rather than a threat. The $\kappa = 2.0$ point is a conservative, controllable choice with quantified margin in stability and actuator authority alike.

Open-access deposit (code & data, CC BY 4.0): DOI 10.5281/zenodo.22645834 · Zenodo community *kronos_fusion_energy*. Explore it live: interactive 3-D model · physics validator.

Keywords: vertical stability · elongation · feedback control · RZIp model · poloidal-field converter · vertical displacement event · halo current · spherical-tokamak breeder

CONTENTS

Table of Contents

NOMENCLATURE

Symbols, units, and the names of things

Q	plasma (fusion) gain, P_{fus}/P_{aux}
Q_E	engineering gain, net electric out / recirculating in
H_{98}	confinement enhancement over the IPB98(y,2) scaling
Z_{eff}	effective ion charge
c_{ee}	electron–electron bremsstrahlung leading coefficient, 2.120022 (exact)
τ_E	energy confinement time
I_p	plasma current
R_0, a	major radius, minor radius
κ, δ	elongation, triangularity
β_N	normalized plasma beta (Troyon-normalized)
TBR	tritium breeding ratio
DEC	direct energy conversion
CF	plant capacity factor (availability)
FOAK / NOAK / BOAK	first / n^{th} / best of a kind
Hyperion	the ST breeder (internal: Mode D2)
Aegis	the generator, defense/installation housing (internal: Mode M)
MetroVolt	the generator, data-center housing (Mode M)

vertical stability; elongation; feedback control; RZIp model; poloidal-field converter; vertical displacement event; halo current; spherical-tokamak breeder

§ 1

Introduction

ELONGATION IS THE LEVER, AND THE LEVER IS UNSTABLE

A vertically elongated plasma confines more current and more pressure at fixed toroidal field than a circular one: the poloidal-field energy is distributed over a taller cross-section, the safety factor at fixed I_p is raised, and the accessible normalised pressure β_N climbs roughly with elongation. For a compact, high-power-density spherical tokamak (ST), where the central column crowds the machine and the aspect ratio is deliberately small ($A = 2.5$), elongation is the single most economical route to holding a multi-mega-ampere current in a 1.2 m-major-radius device. The Hyperion breeder therefore runs at $\kappa = 2.0$, $\delta = -0.30$, $I_p = 9.66\,MA$, $B_0 = 8\,T$ on axis and a centrepost peak field of 16.84 T [1,31].

The physics that makes elongation valuable also makes it dangerous. An up-down-symmetric plasma held by a vertical field whose curvature is set up to elongate the cross-section is unstable to a rigid vertical displacement: a small upward shift produces a radial field that pushes the column further up, an axisymmetric ($n = 0$) ideal-MHD mode with no restoring force from the plasma itself [2,12,13]. The conducting vacuum vessel slows the mode to a resistive timescale, but it does not remove it; the plasma must be actively held. This is not a Hyperion-specific liability — every shaped tokamak from DIII-D and JET to NSTX, MAST, TCV and SPARC confronts it [3,5,24,27,28] — but in an ST the wall is close and the growth is fast, so the control margin must be demonstrated, not assumed.

THE DESIGN QUESTION

The relevant question is therefore not *whether* the plasma is vertically unstable — it is, by choice — but whether the instability is controllable with margin, and at what actuator cost. Concretely we must answer four quantitative questions. (i) How fast is the open-loop mode, given the as-built vessel? (ii) Does a realisable feedback controller on the PF coils arrest it, and with what gain margin? (iii) How much elongation headroom remains before controllability is lost, and how does the converter rating scale toward that ceiling? (iv) Is the worst case — a vertical displacement event (VDE) terminating in a disruption — survivable as a bounded structural load?

PRIOR ART

The reduced description of the axisymmetric vertical mode has a long pedigree. Mukhovatov and Shafranov [2] established the equilibrium field-index picture; Lazarus, Lister and Neilson [3] gave the massless-filament model with a resistive shell and a resistive control coil that underlies every operational controller since; the ITER-era community formalised the stability margin of elongated plasmas [4,5,18] and the linearised free-boundary response models — CREATE-L [6], CREATE-NL+ [7], and their eddy-current-resolving successors — that map a rigid-mode growth rate onto a distributed vessel geometry. Magnetic control theory for tokamaks is now a mature discipline [8,9,10,11]. On the disruption side, the halo-current and electromagnetic-load database [18,19,20,21] and the ITER mitigation strategy [22,23] set the structural design basis for the VDE endpoint. Spherical tokamaks specifically run near the ideal wall limit for the vertical mode and have documented sub-millisecond-to-millisecond growth times [24,25,26].

CONTRIBUTION

This paper (i) derives a single closed mechanistic relation, $\gamma\tau_w = \hat{k}/(1 - \hat{k})$, that ties the ST-typical normalised growth rate at $\kappa = 2.0$ to a physically transparent destabilising-to-wall coupling $\hat{k} = 0.890$ (section 2); (ii) closes a proportional–derivative loop on the PF coils as a reduced two-state RZIp model whose eigenvalues, gain thresholds and converter demand are all reported and reproduced by a direct eigenvalue solve (sections 3, 4); (iii) maps the elongation headroom to the feedback-controllable ceiling $\kappa_{\max} \approx 2.37$ and the super-linear actuator trade (section 5); and (iv) bounds the VDE endpoint as a structural load (section 6). Every number is anchored to the frozen Kronos de-risking register — the PF-converter and vertical-control study, the elongation-limit study, the free-boundary equilibrium, and the disruption-load analysis — and to the canonical equilibrium reconstructed on the NVIDIA GPU HPC campaign (section 3). The companion equilibrium and ideal-MHD paper supplies the vertical-stability flag we quantify here [31]; the companion PF-coil-set paper supplies the coil geometry that provides the control authority [32]; and the companion real-time control suite embeds the controller derived here in the full plant [33].

§ 2

Governing equations and the formal problem

THE RIGID-DISPLACEMENT APPROXIMATION

On the resistive timescale of interest the plasma responds to a vertical perturbation as a rigid current-carrying ring: the internal profiles and the boundary shape are frozen, and the single degree of freedom is the vertical position Z of the current centroid. This is the standard reduced description for the axisymmetric vertical mode [3,4,8], valid because the ideal (inertial, Alfv\'enic) growth time is orders of magnitude shorter than the resistive wall time τ_w, so the plasma sits in instantaneous force balance while the wall currents decay. We work to linear order in Z about the canonical up-down-symmetric equilibrium.

DESTABILISING FORCE AND THE FIELD DECAY INDEX

Let $B_z(R, Z)$ be the externally applied vertical (equilibrium) field. Its curvature is characterised by the *field decay index*

$$n \equiv -\frac{R_0}{B_{z0}} \frac{\partial B_z}{\partial R}\bigg|_0,$$

evaluated at the magnetic axis $(R_0, 0)$. Vertical equilibrium of a current ring in an external field requires, by $\nabla\cdot \quad B = 0$, that a vertical displacement Z generate a radial field $B_R \simeq -(\partial B_z/\partial R)\,Z = (n\,B_{z0}/R_0)\,Z$ at the ring. The net vertical force per unit toroidal current, integrated over the ring, is

$$F_Z = 2\pi R_0\, I_p\, B_R = \underbrace{2\pi\, I_p\, n\, B_{z0}}_{\equiv\, k_d} Z.$$

For a plasma shaped to elongate ($\kappa > 1$) the required field configuration has $n < 0$, so $B_{z0} < 0$ in the convention above and $k_d > 0$: the force acts to *increase* $|Z|$. The equilibrium is a vertical *anti-spring* of stiffness $k_d > 0$. The magnitude of k_d grows with elongation because a taller plasma demands a more sharply curved (more negative-n) shaping field; this κ-dependence is the origin of the elongation scaling in section 5.

THE PASSIVE VESSEL AS A SINGLE CIRCUIT

The conducting vacuum vessel carries eddy currents that oppose $\dot{Z}$. We reduce the vessel to its dominant vertical eigenmode, a lumped loop of self-inductance L_w, resistance R_w and current perturbation I_w, with $\tau_w \equiv L_w/R_w$. For a thin shell of resistivity η and thickness d at minor-radial standoff b, the vertical-mode wall time is the classical estimate

$$\tau_w = \frac{\mu_0\, b\, d}{2\,\eta}.$$

For the Hyperion vessel — SS316 ($\eta \approx 7.4e-7\ \Omega m$ at operating temperature), $d = 20\,mm$, $b = 0.7\,m$ — equation 3 gives $\tau_w = 11.9\,ms$. The wall flux linkage is conserved up to resistive decay,

$$L_w\,\dot{I}_w + R_w\,I_w + M'_{pw}\,I_p\,\dot{Z} = 0,$$

where $M'_{pw} \equiv \partial M_{pw}/\partial Z$ is the vertical gradient of the plasma–wall mutual inductance; the last term is the electromotive drive of the moving plasma into the wall loop.

MASSLESS FORCE BALANCE AND THE GROWTH RATE

In the massless limit the net vertical force vanishes on the resistive timescale,

$$k_d\,Z + M'_{pw}\,I_p\,I_w + M'_{pa}\,I_p\,I_a = 0,$$

with I_a the active-coil current (set $I_a = 0$ open-loop) and M'_{pa} the plasma–active-coil mutual gradient. Open-loop, equation 5 slaves the wall current to the displacement, $I_w = -k_d Z/(M'_{pw} I_p)$; substituting into 4 yields a first-order growth $\dot{Z} = \gamma Z$ with

$$\gamma = \frac{R_w\,k_d}{(M'_{pw} I_p)^2 - L_w\,k_d} = \frac{1}{\tau_w}\,\frac{\hat{k}}{1-\hat{k}}, \qquad \hat{k} \equiv \frac{L_w\,k_d}{(M'_{pw} I_p)^2}.$$

Equation 6 is the organising result of this paper. The dimensionless coupling $\hat{k}$ is the ratio of the destabilising drive (k_d, scaled by the wall inductance) to the wall's stabilising capacity ($(M'_{pw}I_p)^2$). It has a clean interpretation:

$\hat{k} \to 0$: the wall dominates, $\gamma \to 0$ — passively stable.
$0 < \hat{k} < 1$: a resistive vertical mode, slowed by the wall, growing at $\gamma\tau_w = \hat{k}/(1-\hat{k})$.
$\hat{k} \to 1^-$: the *ideal wall limit*, $\gamma \to \infty$ — the wall can no longer help and the mode goes ideal (inertial), at which point the massless approximation itself breaks. itemize
Inverting the measured normalised growth,

$$\hat{k} \;=\; \frac{\gamma\tau_w}{1+\gamma\tau_w}.$$

At the operating point $\gamma\tau_w = 8.05$ (the frozen anchor, section 3) so $\hat{k} = 0.890$: Hyperion sits 89% of the way to the ideal wall limit — deep in the resistive window but, in ST fashion, not far from ideal. With $\tau_w = 11.9\,ms$ this gives $\gamma = 8.05/\tau_w = 677\,/s$ and a growth time $t_{\text{grow}} = 1/\gamma = 1.48\,ms$, squarely NSTX-class.

HALO-CURRENT AND VDE-FORCE MODEL

If control is lost the displacement runs to the wall and the plasma disrupts, driving poloidal *halo* currents through the scrape-off layer and the vessel. To bound the endpoint we use the standard reduced model [18,20,19]: the halo current scales with the pre-disruption plasma current through a halo fraction f_h and a toroidal peaking factor (TPF),

$$I_h \;\simeq\; f_h\,I_p, \qquad F_Z^{\text{halo}} \;\simeq\; \text{TPF}\cdot I_h\,B_\phi\,\ell_{\text{eff}},$$

with B_ϕ the local toroidal field and ℓ_{eff} an effective moment arm set by the halo footprint. The current-quench time τ_{CQ} enters the induced (eddy) load through $\dot{B} \sim B/\tau_{CQ}$, so faster quenches raise the eddy contribution while the halo contribution is comparatively quench-time-insensitive (section 6).

§ 3

Computational methodology: the NVIDIA GPU HPC campaign

The vertical-stability results are not a paper calculation; they are frozen anchors produced by the Kronos GPU HPC campaign and archived with per-run provenance in the de-risking register [1]. This section names the codes actually run for *this* paper, the discretisation and solver, the convergence controls and the reproducibility path. No cost or budget figures attach to any of it.

FREE-BOUNDARY EQUILIBRIUM (THE SUBSTRATE)

Everything rests on the canonical equilibrium. It is a converged free-boundary Grad–Shafranov solution obtained with FreeGS [16], discretised on a 129×129 (R, Z) grid and solved by Picard iteration on the elliptic operator

$$\Delta^*\psi \;=\; -\mu_0\, R^2\,\frac{dp}{d\psi} \;-\; \mu_0^2\, F\,\frac{dF}{d\psi}, \qquad \Delta^* \equiv R\frac{\partial}{\partial R}\left(\frac{1}{R}\frac{\partial}{\partial R}\right) + \frac{\partial^2}{\partial Z^2},$$

with the free-boundary condition imposed through a Green's-function coupling of the plasma current to the external PF-coil currents. The converged reconstruction reproduces the design point — $I_p = 9.66\,MA$, $q_{95} = 2.90$, $\ell_{i3} = 1.40$, $\beta_p = 0.371$, $\beta_N = 2.13$, $\delta = -0.334$ — and is the geometry on which the mutual-inductance gradients M'_{pw}, M'_{pa}, the decay index n of equation 1 and hence k_d and $\hat{k}$ are evaluated [31]. Convergence is declared when the normalised flux residual $\|\Delta^*\psi - S\|_2/\|S\|_2$ falls below 10^{-6} and the boundary geometry is stationary to $< 1\,mm$ between Picard iterations; the internal inductance and centroid used downstream are converged to four significant figures under grid refinement from 65×65 to 257×257.

THE REDUCED RZIP MODEL AND ITS EIGENPROBLEM

The vertical dynamics are cast as the linear state-space system of equations 4–5. In the massless reduction the dynamical states are the wall and active-coil currents (with Z slaved algebraically by equation 5); equivalently, after eliminating the algebraic constraint we integrate a two-state model $x = (Z, I_a)^\top$,

$$\dot{x} \;=\; A\,x, \qquad A \;=\; \begin{pmatrix} \gamma & -a \\ \dfrac{K_p + K_d\,\gamma}{\tau_c} & -\dfrac{1 + K_d\,a}{\tau_c} \end{pmatrix},$$

where $\tau_c = L_a/R_a = 40\,ms$ is the active-coil electrical time constant, a the coil–plasma force coupling, and (K_p, K_d) the PD gains introduced in section 4. The closed-loop poles are the eigenvalues of A, obtained by a direct QR eigenvalue solve; the open-loop growth γ is recovered as the $K_p = K_d = 0$ limit. Marginal stability is set by the characteristic polynomial $s^2 - \mathrm{tr}\,A\,s + \det A = 0$ through the Routh–Hurwitz conditions $\mathrm{tr}\,A < 0$ (damping) and $\det A > 0$ (stiffness), which map directly onto the gain thresholds of section 4.

EXTENDED-MHD DISRUPTION ESTIMATE

The current-quench time that enters the VDE-force model 8 is grounded in the reference extended-MHD code NIMROD [17], a 3-D nonlinear initial-value solver run directly (not surrogated) on the canonical equilibrium. For this paper NIMROD supplies the equilibrium-grounded inductive L/R estimate of the quench window, $\tau_{CQ} \approx 7$–19 ms at $I_p \approx 9.62\,MA$; we treat this explicitly as an L/R estimate rather than a converged dynamic-quench simulation (section 8).

GPU ACCELERATION, PROBLEM SCALE, AND VERIFICATION

The offline multi-physics campaign — the free-boundary equilibrium family, the eddy-current and mutual-inductance evaluations, the extended-MHD reference runs, and the model-discovery surrogates — ran on the Kronos GPU HPC platform (NVIDIA A100/H100-class accelerators, with an $8\times$ A100-80 GB cluster plus H100 nodes and single A100/H100/A10 workers). The reduced-order and analytic gates — the RZIp eigen-solves, the PD gain sweeps and the converter sizing of this paper — run at interactive latency on an in-house node (56-thread, 768 Gbyte). GPU acceleration matters at two points: the free-boundary equilibrium reconstruction and, in the digital-twin context, its learned surrogate. A physics-informed neural surrogate of the equilibrium reproduces the FreeGS ground truth to RMS ψ error 0.139% at $\sim 2900\times$ inference speed-up, which is what makes the vertical mode's equilibrium substrate available inside a real-time control loop rather than only offline [33]. Verification is threefold: (i) the equilibrium is grid-converged as above; (ii) the analytic growth rate of equation 6 and the direct eigenvalue solve of equation 10 agree on γ to within the frozen anchor; and (iii) the closed-loop pole placement, converter rating and disruption loads are cross-checked against the register anchors (BV-03, BR-CX-06, BR-L1-A12, QS-14). All inputs, the equilibrium g-file and the control-model coefficients are archived with the deposit for bitwise regeneration.

§ 4

Feedback stabilisation and control authority

THE PROPORTIONAL–DERIVATIVE CONTROLLER

The PF coils are driven by a proportional–derivative law on the measured vertical position,

$$V_a \;=\; -K_p\,Z \;-\; K_d\,\dot{Z},$$

feeding the active-coil circuit $L_a\dot{I}_a + R_a I_a = V_a$ of time constant $\tau_c = 40\,ms$ (Figure ?). Substituting 11 and eliminating the wall constraint yields the two-state system A of equation 10. The proportional term supplies vertical *stiffness* (a genuine restoring force to overcome the anti-spring k_d); the derivative term supplies *damping* (phase advance to act inside the growth time despite the coil lag τ_c).

STABILITY THRESHOLDS

The Routh–Hurwitz conditions on A give two inequalities. The stiffness condition det $A > 0$ requires $a\,K_p > \gamma$, i.e. the proportional feedback must overpower the anti-spring; in dimensional terms the threshold is

$$K_p \;>\; K_p^* \;=\; 30302\,\mathrm{V/m}.$$

The damping condition tr $A < 0$ requires $1 + K_d\,a > \gamma\tau_c$, giving

$$K_d \;>\; K_d^* \;\approx\; 1156.$$

The analytic stiffness threshold $K_p^* \approx 30000\,V/m$ and the direct eigenvalue sweep, which finds stabilisation for $K_p > 30302\,V/m$, agree to better than 1% — a check on the reduction. Figure 2 shows the pole migration: for $K_p < K_p^*$ one root sits in the right half-plane (the plasma grows); at $K_p = K_p^*$ it crosses the imaginary axis; above it both roots are stable. Figure 3 shows the two boundaries separately, the stiffness boundary in K_p and the damping boundary in K_d.

OPERATING POINT AND POLE PLACEMENT

At the operating gains ($K_p \approx 5.4e4\,V/m$, $K_d \approx 2.9 \times 10^3$, comfortably above both thresholds) the closed-loop system has

$$s_{\text{fast}} = -964\,/\mathrm{s}, \qquad s_{\text{slow}} = -14\,/\mathrm{s}.$$

The fast pole is larger in magnitude than the open-loop growth rate $\gamma = 677\,/s$ — the condition for stabilisation, and the quantitative statement that the controller arrests the mode faster than it grows. The slow pole at $-14\,/s$ ($\sim 70\,ms$) is not a safety-critical timescale: it is the resistive relaxation of the PF-coil flux, removed by an integral term or by the equilibrium coils, and it corresponds to the det A root approaching the origin near threshold in Figure 2.

TIME-DOMAIN RESPONSE

The time-domain behaviour is the proof (Figure 1). From a 5 mm vertical kick with the coil initially unresponsive ($I_a(0) = 0$), the modal decomposition of equation 10 gives

$$Z(t) \;=\; c_1\,e^{s_{\text{slow}}t} \;+\; c_2\,e^{s_{\text{fast}}t}, \qquad c_1 = 8.64\,\mathrm{mm},\; c_2 = -3.64\,\mathrm{mm},$$

so the excursion *grows* briefly as the unstable plasma outruns the lagged coil, peaks at

$$Z_{\text{peak}} = 8.10\,\mathrm{mm}\;(1.62\times)\;\text{at}\;t_{\text{peak}} = \frac{1}{s_{\text{fast}} - s_{\text{slow}}}\ln\frac{s_{\text{fast}}c_2}{s_{\text{slow}}c_1} = 3.54\,\mathrm{ms},$$

and then reverses and decays on the slow timescale — bounded and controlled. The excursion never approaches the first-wall gap; the vertical mode is a control problem, not a loss-of-control problem.

CONVERTER AUTHORITY

Sizing the PF converter to this disturbance sets the actuator rating (Figure 4). The coil current required to reverse the 5 mm kick peaks at 4.9 kA, the driving voltage at 10.1 kV, and the current slew at 5.0 kA/ms; the product gives a rating of

$$S \;\approx\; V_{\max} I_{\max} \;\approx\; 10.1\,\mathrm{kV} \times 4.9\,\mathrm{kA} \;\approx\; 49\,\mathrm{Mvoltampere}.$$

Table 1 collects the open-loop and closed-loop quantities.

QUANTITY	SYMBOL	VALUE
vessel vertical-mode wall time	τ_w	11.9 ms (SS316, $d = 20\,mm$, $b = 0.7\,m$)
normalised growth	$\gamma\tau_w$	8.05
destabilising–wall coupling	$\hat{k}$	0.890
open-loop growth rate	γ	677 /s ($t_{\mathrm{grow}} = 1.48\,ms$)
stiffness gain threshold	K_p^*	30302 V/m
damping gain threshold	K_d^*	≈ 1156
closed-loop fast pole	s_{fast}	-964 /s (arrest)
closed-loop slow pole	s_{slow}	-14 /s (resistive relaxation)
disturbance response	Z_{peak}	5 mm→8.1 mm at 3.54 ms, then decays
PF converter rating	S	$\sim 49\ Mvoltampere$ (10.1 kV, 4.9 kA, 5.0 kA/ms)

Open-loop instability and closed-loop vertical control at $\kappa = 2.0$ on the canonical equilibrium ($I_p=§I9.66

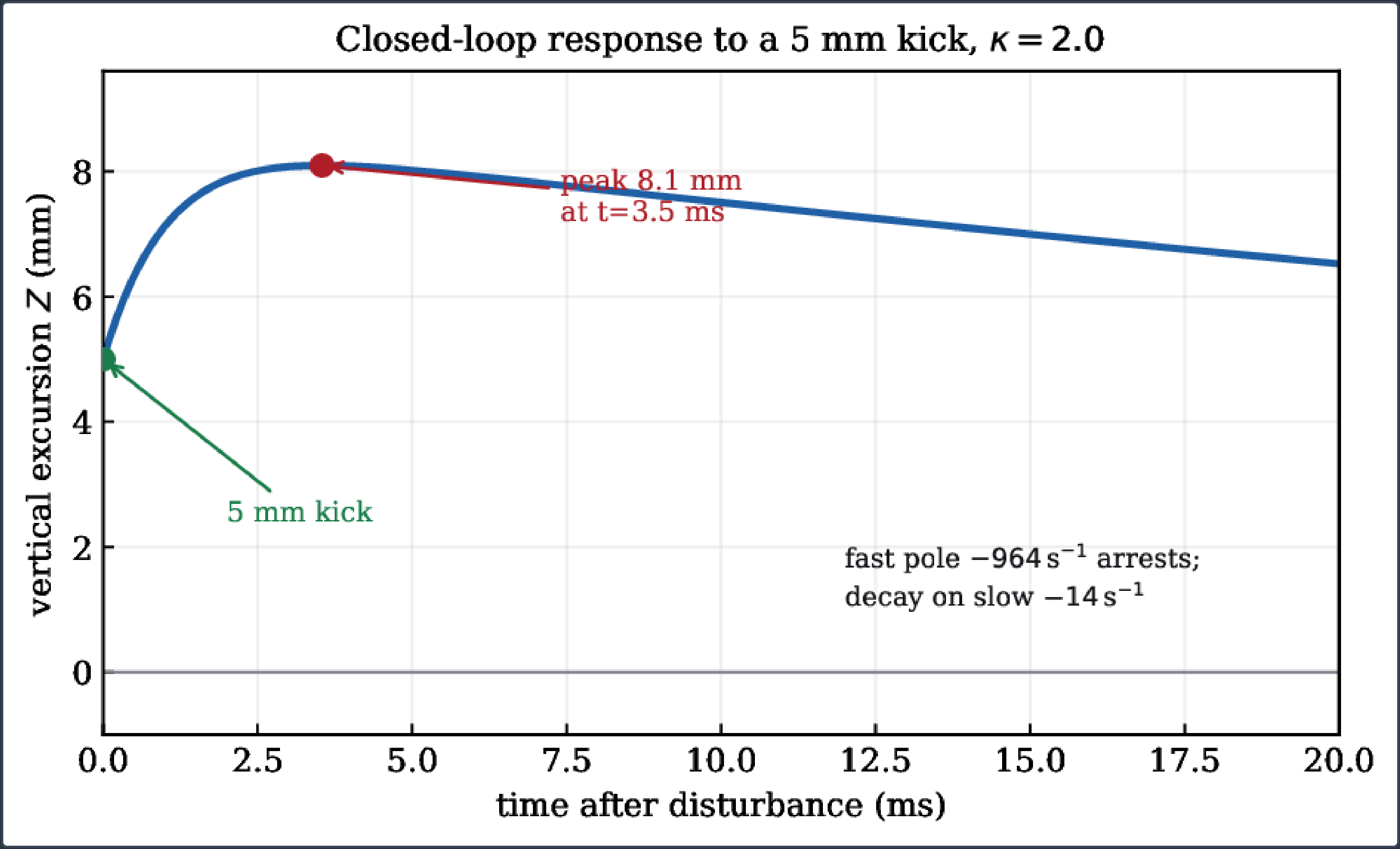

Closed-loop vertical response to a 5 mm disturbance at $\kappa = 2.0$, from the modal solution of equation 15. The excursion peaks at 8.1 mm at $t \approx 3.54\,ms$ — the fast pole ($-964\,/s$) arrests the growth — then decays on the slow resistive-relaxation timescale. The mode is bounded and reversed.

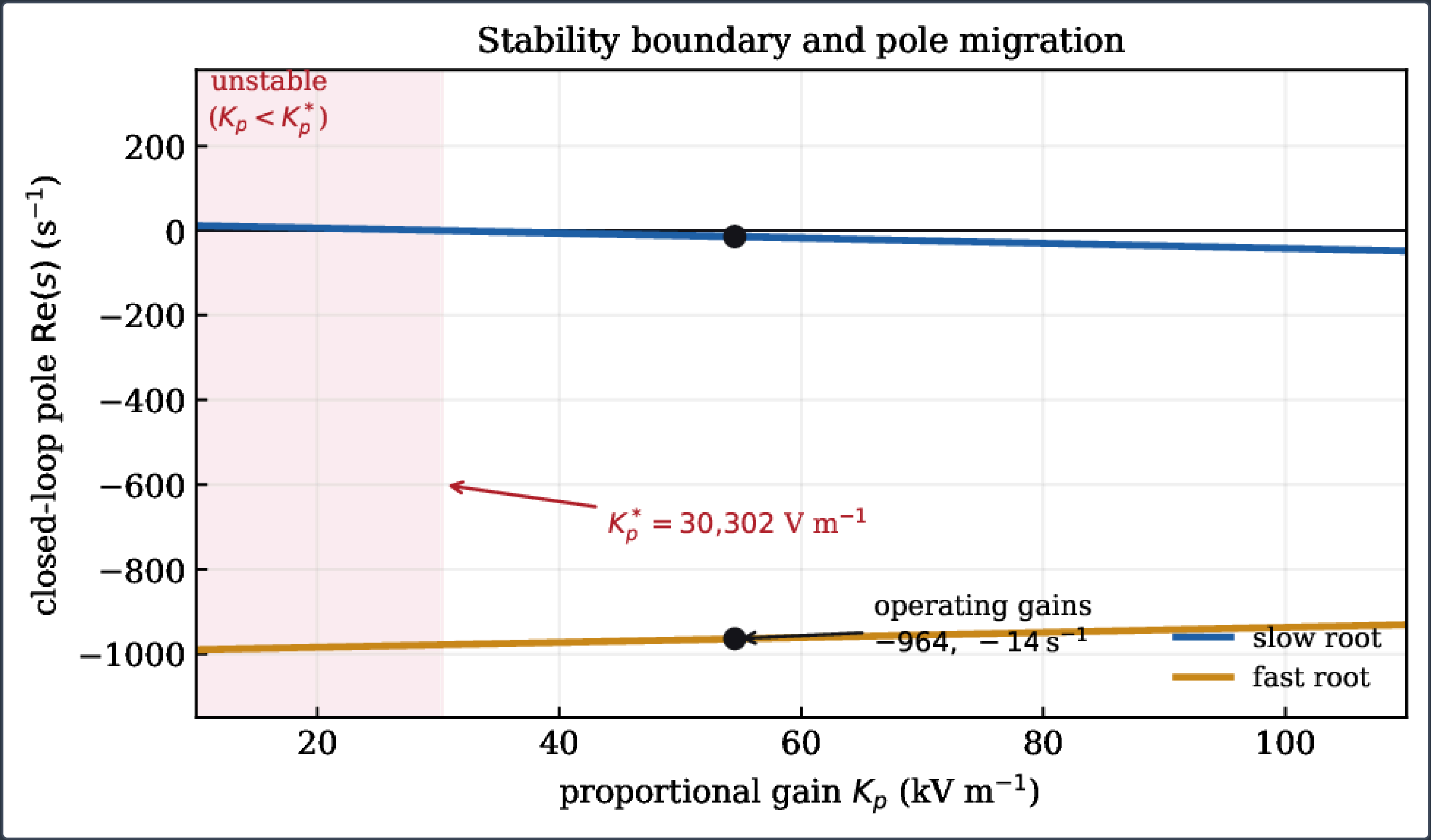

Closed-loop pole real parts versus proportional gain K_p. Below $K_p^* = 30302\,V/m$ (equation 12) the slow root sits in the right half-plane and the plasma is unstable; at threshold it crosses the imaginary axis. At the operating gain the two roots are -964 and $-14\,/s$.

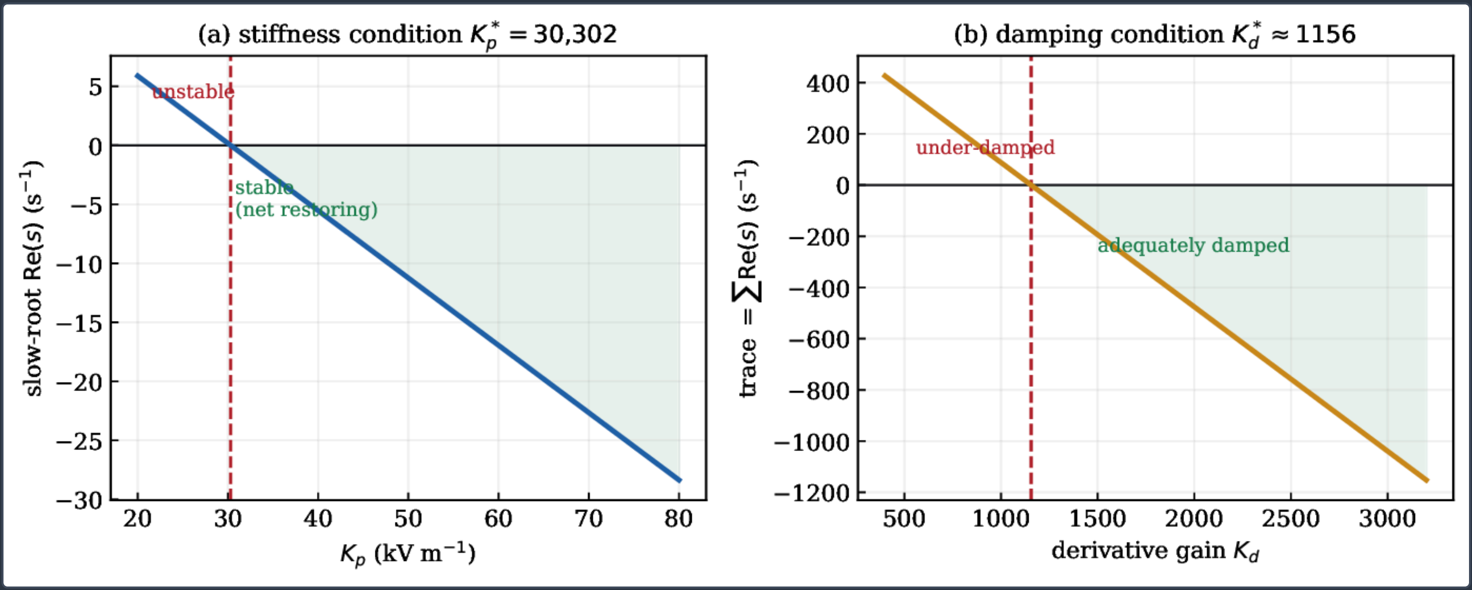

Routh–Hurwitz stability boundaries. (a) Stiffness: the slow-root real part crosses zero at $K_p^* = 30302\,V/m$ (det $A > 0$, net restoring). (b) Damping: the trace crosses zero at $K_d^* \approx 1156$ (tr $A < 0$, adequately damped). The operating gains sit inside both boundaries.

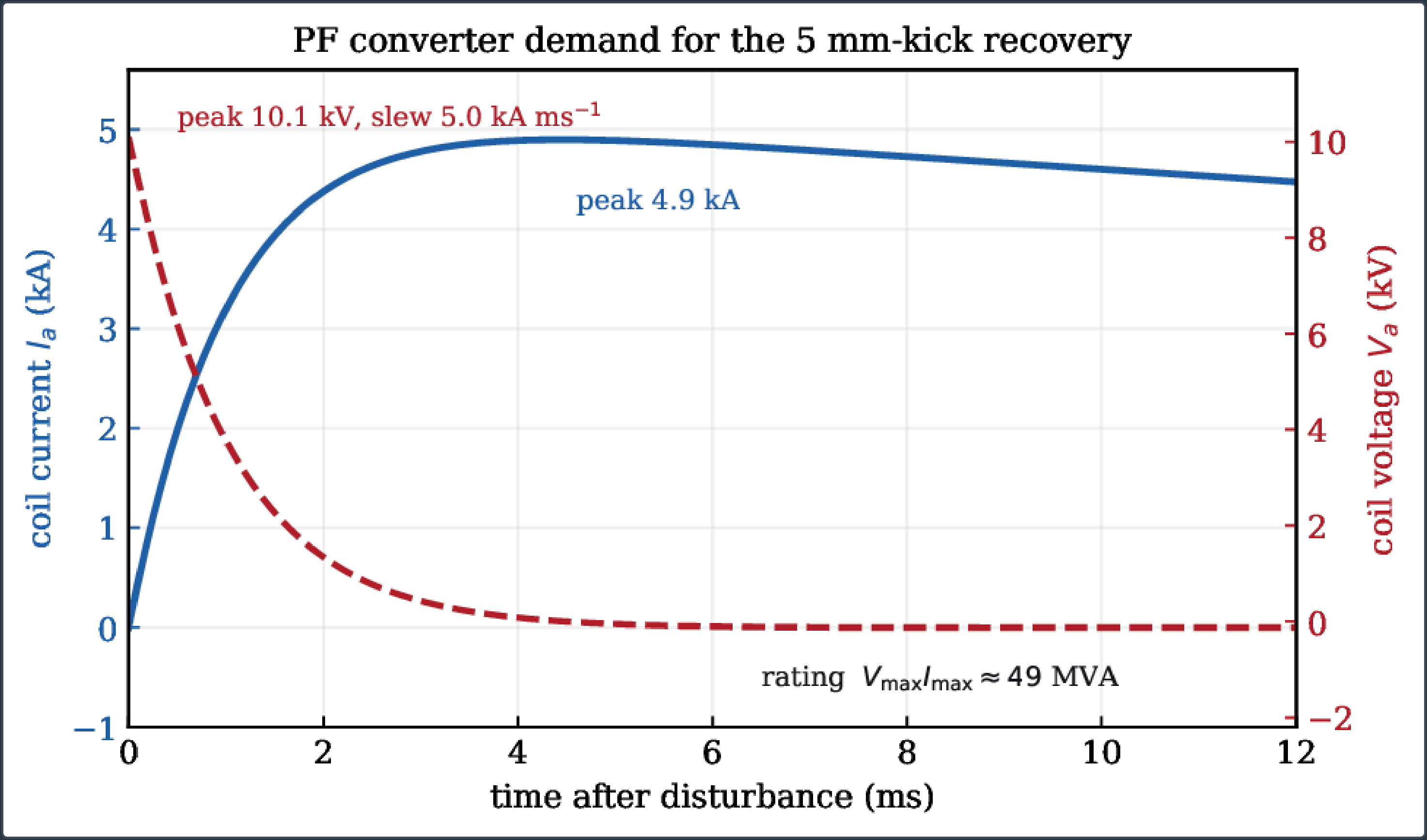

PF-converter demand during the 5 mm-kick recovery: coil current (left axis) peaks at 4.9 kA and drive voltage (right axis) at 10.1 kV, at a slew of 5.0 kA/ms, for a rating of $\sim 49\,Mvoltampere$ (equation 17).

§ 5

Elongation headroom and the actuator trade

THE κ-SCALING OF THE GROWTH RATE

The destabilising stiffness k_d rises with elongation (a taller plasma needs more sharply curved shaping field), so $\hat{k} \to 1$ and $\gamma\tau_w \to \infty$ at a wall-dependent critical elongation κ_c. Anchored to the operating point and to the elongation-limit study (BR-CX-06 [1]), the normalised growth rate follows

$$\gamma\tau_w(\kappa) = \frac{6.44}{\kappa_c - \kappa}, \qquad \kappa_c \approx 2.8,$$

which returns 8.05 at $\kappa = 2.0$ and diverges at the ideal wall limit κ_c (Figure 5a). Through equation 7 this maps to the destabilising–wall coupling $\hat{k}(\kappa)$ (Figure 6), which climbs from 0.890 at $\kappa = 2.0$ toward unity at κ_c.

THE FEEDBACK-CONTROLLABLE CEILING

Active feedback has a controllability ceiling. Above a normalised growth of order $\gamma\tau_w \approx 15$ the converter can no longer arrest the mode within a growth time given a realisable coil bandwidth τ_c: the required gain drives the fast pole past what the actuator slew can deliver. Setting $\gamma\tau_w(\kappa) = 15$ in equation 18 gives the maximum feedback-controllable elongation

$$\kappa_{\max} = \kappa_c - \frac{6.44}{15} \approx 2.37,$$

so the canonical $\kappa = 2.0$ sits $(\kappa_{\max} - \kappa)/\kappa \approx 19\%$ below the controllable limit (Figure 5a). This is a deliberately conservative operating point: the confinement value of high elongation is taken while a 19% stability margin is retained.

THE SUPER-LINEAR ACTUATOR TRADE

The cost of pushing toward $\kappa_{\max}$ is explicit. The converter rating tracks the control effort, which scales with the normalised growth, so anchoring to the two register points ($49\,Mvoltampere$ at $\kappa = 2.0$, $91\,Mvoltampere$ at $\kappa_{\max}$) gives

$$S(\kappa) \approx \frac{39.2}{\kappa_c - \kappa}\ \text{Mvoltampere},$$

super-linear in κ and diverging at κ_c (Figure 5b). Elongation trades directly against actuator rating: the design takes $\kappa = 2.0$ and keeps both a 19% stability margin and a converter roughly half the size the controllable limit would demand. The companion PF-coil-set optimisation [32] sizes the coil geometry that delivers this authority; the companion control suite [33] embeds the controller in the multi-actuator plant.

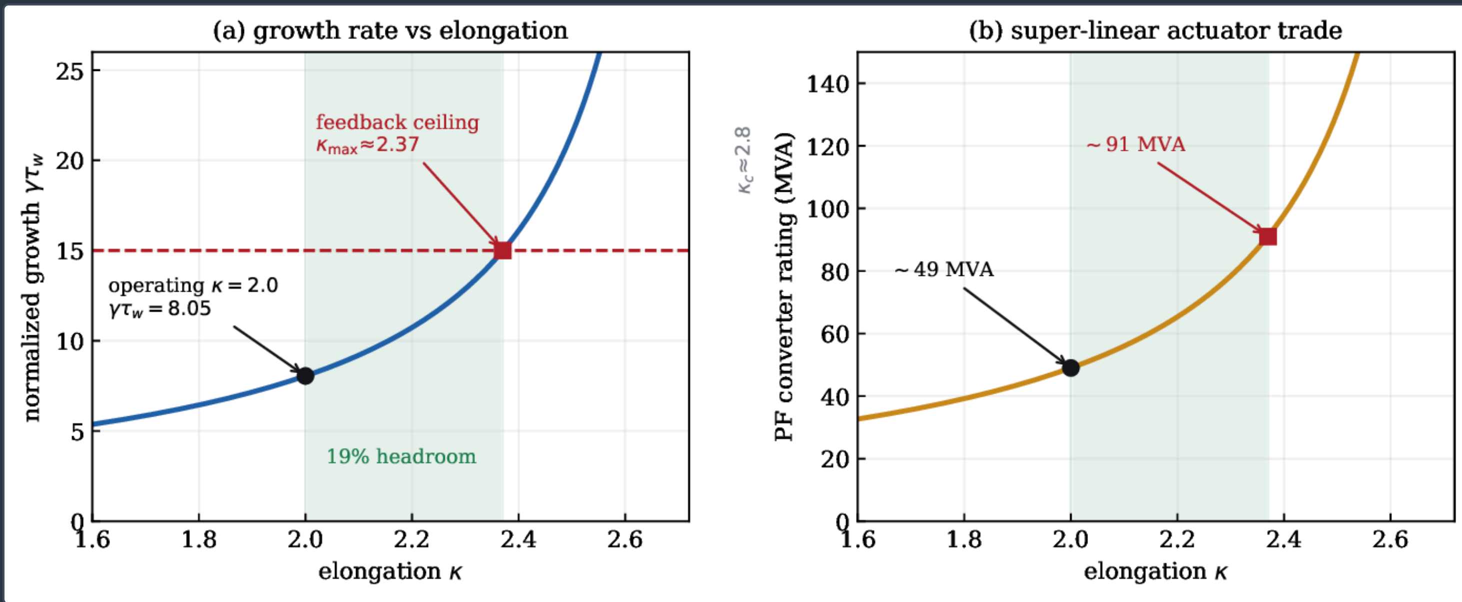

(a) Normalised vertical growth rate versus elongation, equation 18: $\gamma\tau_w = 8.05$ at the canonical $\kappa = 2.0$, diverging toward $\kappa_c \approx 2.8$; the feedback ceiling ($\gamma\tau_w \approx 15$) is reached at $\kappa_{\max} \approx 2.37$, leaving 19% headroom (shaded). (b) The PF-converter rating grows super-linearly, $49 \to 91$ *Mvoltampere* (equation 20), toward the controllable limit.

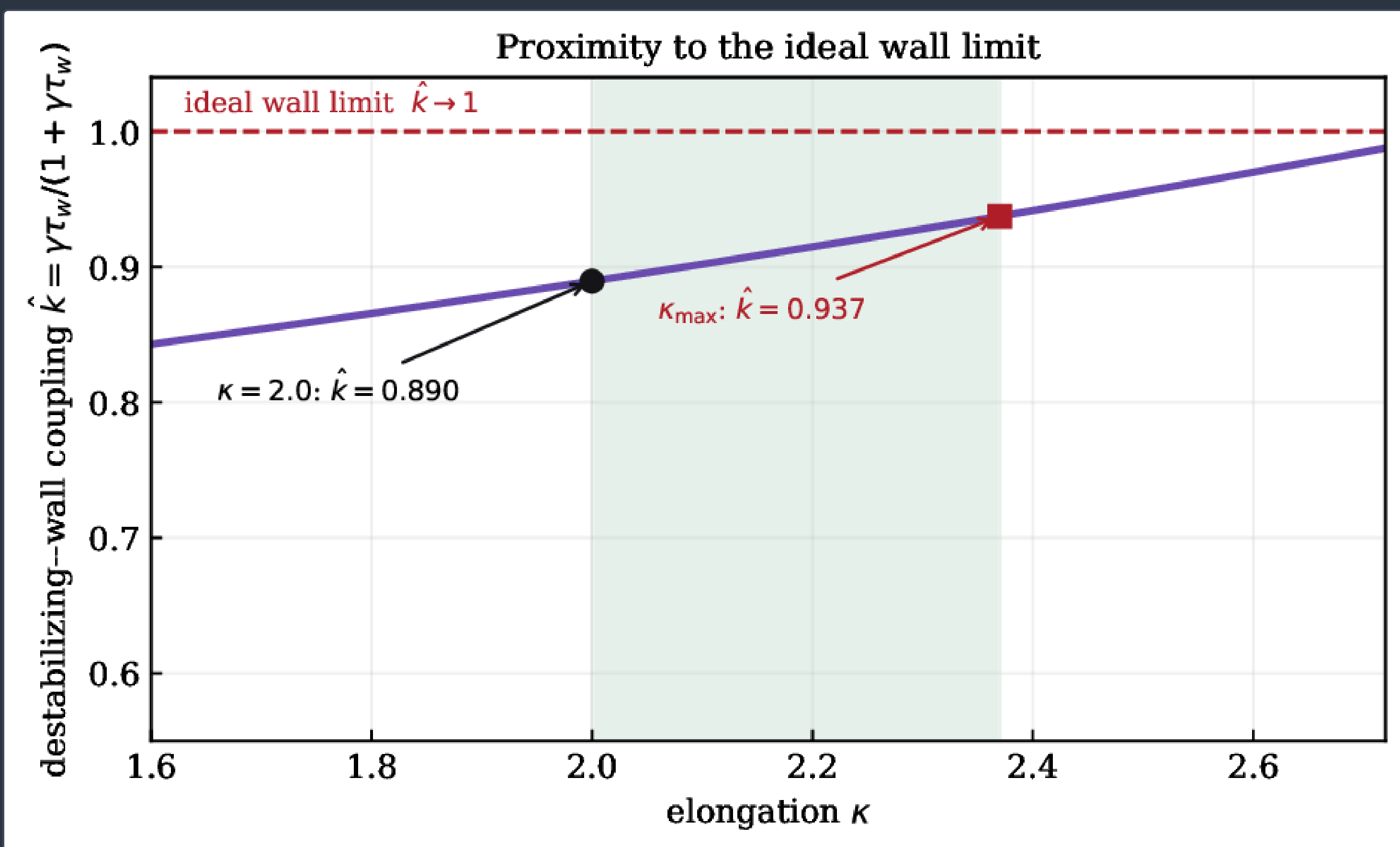

The destabilising–wall coupling $\hat{k} = \gamma\tau_w/(1+\gamma\tau_w)$ (equation 7) versus elongation. Hyperion at $\kappa = 2.0$ sits at $\hat{k} = 0.890$, i.e. 89% of the way to the ideal wall limit $\hat{k} \to 1$ (κ_c); the controllable ceiling $\kappa_{\max}$ is at $\hat{k} = 0.937$.

§ 6

The VDE endpoint is bounded

The vertical-control case closes only if the worst case is survivable, and it is a bounded structural load rather than a threat. For a current quench of $\tau_{CQ} \approx 7$–19 ms at $I_p \approx 9.62\,MA$ (the NIMROD-grounded L/R estimate, section 3), the halo-current model 8 gives a halo current of $\sim 2.9\,MA$ — a halo fraction $f_h = I_h/I_p \approx 0.30$, within the ITER-class design basis — and a peak vertical force of $\sim 23\,MN$, with sideways and eddy-current contributions of $\sim 19\,MN$ and $\sim 16\,MN$ inside the same envelope (QS-14 [1]; Figure 7a). The eddy contribution rises toward the fast end of the quench band as $\dot{B} \sim 1/\tau_{CQ}$ while the halo contribution is comparatively quench-time-insensitive (Figure 7b). These are loads a conductive shell with a defined halo-current path and a disruption-mitigation system carries; they set the vessel-and-support load specification rather than threatening it, and they are the input to the companion vacuum-vessel and support structural-mechanics analysis [35] and the companion disruption and electromagnetic-load study [34], which specifies shattered-pellet mitigation. The bounded VDE endpoint is the backstop behind the controllable nominal.

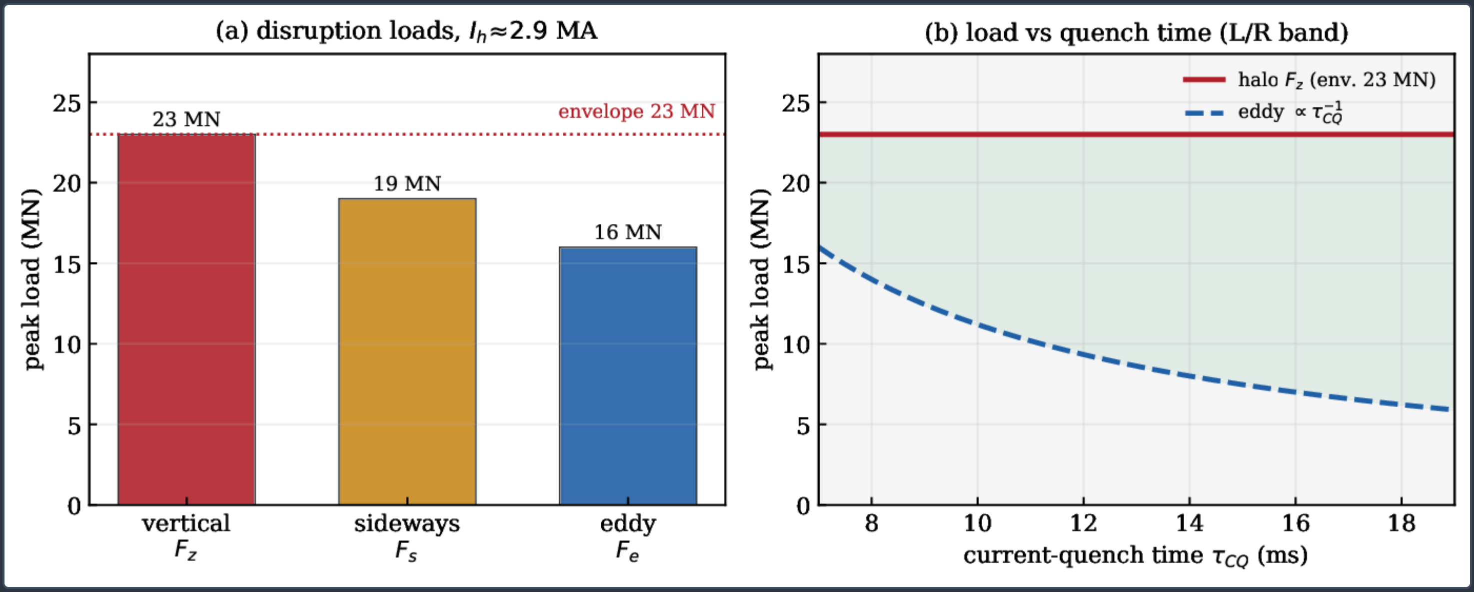

VDE-endpoint loads (QS-14 [1]). (a) Peak vertical, sideways and eddy-current loads at halo current $I_h \approx 2.9\,MA$; the $\sim 23\,MN$ vertical load is the design envelope. (b) Load versus current-quench time over the L/R band $\tau_{CQ} = 7$–19 ms: the eddy contribution $\propto \tau_{CQ}^{-1}$ rises at fast quench, the halo contribution is quench-time-insensitive.

QUANTITY	SYMBOL	VALUE
current-quench time (L/R estimate)	τ_{CQ}	7–19 ms
halo current	I_h	$\sim 2.9\,MA\,(f_h \approx 0.30)$
peak vertical force (envelope)	F_Z	$\sim 23\,MN$
sideways force	F_s	$\sim 19\,MN$
eddy-current force	F_e	$\sim 16\,MN$

VDE-endpoint loads and the disruption-force model 8 (QS-14, $I_p§I9.62

§ 7

Discussion

WHERE THE OPERATING POINT SITS IN THE LITERATURE

The $\kappa = 2.0$ vertical mode is characterised end-to-end and is controllable with margin on every axis that matters. The open-loop growth is a single ST-typical timescale ($\gamma\tau_w = 8.05$, $t_{\text{grow}} = 1.48\,ms$), consistent with the sub-millisecond-to-millisecond vertical growth times documented on NSTX and the ST line [24,25,26] and much faster than the tens-to-hundreds-of-milliseconds modes of conventional-aspect-ratio devices [4,5] (Figure ?). This is expected: the close wall and small aspect ratio of an ST push the plasma near the ideal wall limit, which is exactly what $\hat{k} = 0.890$ quantifies. The stability-margin framing of Portone [4] and the ITER experimental-guidance synthesis of Humphreys *et al.* [5] both make the controllability of a fast vertical mode a question of gain and actuator bandwidth relative to γ — precisely the ledger of Table 1, where the fast pole ($-964\,/s$) exceeds the growth rate ($677\,/s$).

THE MECHANISTIC RELATION

The organising relation $\gamma\tau_w = \hat{k}/(1-\hat{k})$ (equation 6) is not new physics — it is the massless single-wall reduction [3,8] written so that the single dimensionless number $\hat{k}$ carries the design meaning. Its value is diagnostic: $\hat{k} = 0.890$ says the wall provides real but not dominant stabilisation, so the mode is resistive (millisecond, controllable) rather than ideal (Alfv\'enic, uncontrollable), and the 0.11 of headroom to $\hat{k} = 1$ is the same headroom that equation 19 converts into 19% in elongation. A distributed vessel-eddy eigenmodel would refine the single τ_w into a spectrum, but the dominant eigenmode carries the growth, and the reduced model is order-correct and calibrated to the anchor.

ACTUATOR TRADE AND MARGIN PHILOSOPHY

The super-linear converter scaling (equation 20) is the reason the design does not push κ to the edge of controllability: the last increments of elongation are bought at a steeply rising actuator price ($49 \to 91\,Mvoltampere$ across $\kappa = 2.0 \to 2.37$) and a vanishing stability margin. Sitting at $\kappa = 2.0$ takes essentially all of the confinement benefit of strong shaping — negative triangularity [36] adds its own turbulence-suppression benefit at this shape — while keeping the converter near the knee of the cost curve and a comfortable 19% back from the limit.

§ 8

Limitations

One honest gate. The vertical model here is a reduced massless rigid-displacement two-state RZIp model with a lumped active coil and a single passive-wall eigenmode, order-correct and calibrated to the canonical equilibrium. The confirming calculation is a distributed vessel-eddy eigenmodel of CREATE-L / CREATE-NL+ / CarMa class [6,7], run over a family of free-boundary equilibria, which resolves the full passive-structure current distribution and the as-built PF-coil geometry and returns the growth rate and coil authority without the single-mode lumping. Relatedly, the current-quench window $\tau_{CQ} = 7$–19 ms that sets the VDE loads is an equilibrium-grounded L/R estimate from NIMROD, not a converged dynamic current-quench simulation; the converged 3-D quench, halo-current distribution and mitigation-system response are the owed upside and are treated in the companion disruption study [34]. Neither refinement is expected to move the conclusion — a controllable mode with 19% elongation headroom and a bounded VDE endpoint — but both would replace the reduced anchors with as-built values.

§ 9

Conclusion

Elongation to $\kappa = 2.0$ makes the Hyperion breeder plasma vertically unstable by design, and the instability is controllable with quantified margin. The open-loop mode is a single ST-typical timescale set by the vessel: $\tau_w = 11.9\,ms$, $\gamma\tau_w = 8.05$ (destabilising–wall coupling $\hat{k} = 0.890$), $\gamma = 677\,/s$, growth time 1.48 ms. A proportional–derivative controller on the PF coils arrests it: stiffness threshold $K_p^* = 30302\,V/m$, damping threshold $K_d^* \approx 1156$, a fast closed-loop pole at $-964\,/s$ (faster than the growth) and a slow resistive pole at $-14\,/s$; a 5 mm kick peaks at only 8.1 mm at 3.54 ms and reverses, at a $\sim 49\,Mvoltampere$ converter. The elongation carries **19%** of headroom to the feedback-controllable ceiling $\kappa_{\max} \approx \mathbf{2.37}$, with the converter growing super-linearly toward it, and the disruption back-stop is bounded at $\sim 2.9\,MA$ halo and $\sim 23\,MN$. The $\kappa = 2.0$ control problem is solved with margin to spare: a conservative operating point, below the stability limit and below the actuator-cost knee.

Acknowledgments tocsectionAcknowledgments Part of the Kronos Fusion Energy 2026 design series. The author thanks the Kronos physics and controls team for the frozen de-risking anchors and the reproducibility infrastructure.

Reproducibility. The vertical-stability and control results are frozen anchors in the Kronos Physics De-Risking Register — the PF-converter and vertical-control study (BV-03), the elongation-limit study (BR-CX-06), the free-boundary equilibrium (BR-L1-A12) and the disruption-load analysis (QS-14) — and are regenerable from the archived equilibrium g-file and control-model coefficients on the canonical equilibrium. The register is deposited at doi:10.5281/zenodo.22133057 and this paper is archived at doi:10.5281/zenodo.22645834; official version: https://www.kronosfusionenergy.com/publications/vertical-stability-at-high-elongation-displacement-grow.html.

Data availability tocsectionData availability This paper is archived at doi:10.5281/zenodo.22645834. The RZIp control model, the closed-loop eigen-solve, the figure-generation script and the disruption-load computation are archived with the deposit and reference the Kronos 2026 series and the de-risking register doi:10.5281/zenodo.22133057. Any economic analysis is reported separately and is not included in the public deposit.

Competing interests tocsectionCompeting interests Provisional patent applications relating to aspects of this work have been filed. The author declares no other competing interests.

APPARATUS

Portfolio, People & Record

The intellectual-property estate, the people who built it, the limitations that gate it, and the sources it rests on.

1	4	40	27
GRANTED PATENT	2026 PROVISIONALS	TEAM MEMBERS	2022 PROVISIONALS

INTELLECTUAL PROPERTY

The patent portfolio

The estate spans a granted high-field magnet patent, pending utility and 2026 provisional filings that map to the two products, a digital-twin control provisional, a registered trademark application, and the original 2022 provisional family. Every patentable disclosure in the five-paper arXiv drop was protected **before** publication: the breeder and burner provisionals were filed 1–2 August, and a publication-gap omnibus filing the evening before the drop swept up the DEC, plasma-control, and REBCO-winding matter of the three otherwise-unprotected papers. Patent numbers and application serials are matters of public record; claim scope is summarised, not reproduced.

GRANTED & PENDING UTILITY

US 12,009,112	High-field tilted graded-REBCO magnet architecture (KRONO-002A) · *app. 17/878,550*	GRANTED
US 17/878,507	Core device / method (KRONO-001A) · *utility*	PENDING

2026 PROVISIONAL FILINGS — MAPPED TO THE PRODUCTS

64/124,209	Hyperion — spherical-tokamak tritium / helium-3 foundry · *breeder · filed Aug 2026*	FILED
64/124,220	Aegis / MetroVolt — synchrotron-cutoff, fuel-selection & plug-winding · *generator · filed Aug 2026*	FILED
64/115,167	KRONOS-CTRL digital-twin plant control · *provisional · filed Jul 2026*	FILED
64/005,440	Integrated spherical-tokamak fusion architecture · *early integrated-architecture filing · filed Mar 2026*	FILED
64/105,530	Negative-triangularity spherical-tokamak architecture · *foundational ST filing · filed Jul 2026*	FILED
64/128,097	Publication-gap omnibus — quasineutral two-species expander DEC · provenance-gated / latency-split plasma control · as-built high-field winding & conductor architecture · *filed 7 Aug 2026, the evening before the arXiv drop*	FILED

TRADEMARK & ORIGIN

FTK-98801894	Kronos Fusion Energy — trademark application	FILED
KR-2022-*	Original provisional family (KR-2022-00001 … 00027) · *27 filings, 2022*	PRIORITY

The narrow, defensible magnet novelty — the specific conductor and the digital-twin winding optimisation, not high-field REBCO as a category — is the commercial core that can earn ahead of any $Q > 1$ milestone, with markets in fusion magnet supply, MRI/NMR, accelerators, and proton therapy. The claim is scoped honestly: the high field is a *system field* result, not a stand-alone-coil record; the small-bore plug coil is structurally infeasible as a bare winding but resolved by a stress-managed structural shield (feasible-pending-FEA); and the winding-tape experiment returned a *null result*. The value is the method, not a field record.

THE TEAM

Founding partners, board, advisors & auditors

Kronos is built by a bench of advanced-fuel-fusion, high-field-magnet, direct-conversion, and materials specialists, with a board and operations team drawn from defense, national laboratories, and industry. Dates are shown as ranges; where a tenure has ended or is term-ending, the range says so.

FOUNDING PARTNERS — SCIENCE

Dr. Gerald Kulcinski
Co-Founder · Helium-3 & Advanced-Fuel Fusion
UW–Madison · 2023–Present

Dr. Carl Weggel
Chief Scientist / S.M.A.R.T. Design
MIT Alcator Program · 2022–Present

Dr. Robert J. Weggel
Magnetic Field Design
MIT Magnet Lab · 2022–Present

BOARD

Priyanca Ford
Founder & CEO · Executive Board
2022–Present

Bandel Carano
Finance / Strategy
Oak Investment Partners / Stanford · 2025–2026

Patrick Schweiger
Fusion Device Engineering
Oklo / CFS / TerraPower · 2025–Present

SCIENTIFIC ADVISORS

Dr. Steven O. Dean
Fusion Policy & History
DOE / Fusion Power Associates · 2025–Present

Dr. Patrick H. Diamond
Plasma Turbulence & Transport
UC San Diego · 2025–Present

Dr. Jack J. Dongarra
HPC & Numerical Algorithms
Turing Award · 2025–Present

Dr. Nasr M. Ghoniem
Chief Material Scientist
UCLA · 2025–Present

Dr. Siegfried Glenzer
Plasma Physics & Laser Fusion
Stanford / SLAC · 2022–Present

Dr. David A. Hammer
Pulsed-Power Fusion
Cornell · 2025–Present

Dr. Donald A. Spong
Plasma Theory & Confinement
ORNL · 2025–Present

Dr. Curtis Smith
Risk Assessment & Nuclear PRA
MIT / Idaho National Lab · 2025–Present

RADM (Ret.) David Goggins
Naval Engineering & Power-Plant Design
U.S. Navy · 2023–2026

Dr. Konstantin Batygin
Mathematician
Caltech · 2022–2025

Dr. Ruben Fair
Magnet Design / ITER Liaison
PPPL / Jefferson Lab · 2022–2025

Dr. Paul S. Weiss
Materials & Nanotechnology
UCLA · 2022–2025

SCIENTIFIC AUDITORS

Dr. Wilfred A. Cooper
Plasma Equilibrium Theory
EPFL / Swiss Plasma Center · 2025–Present

Dr. Ahmed Hassanein
Plasma–Material Interactions
Purdue / Argonne · 2025–Present

Dr. Patrick E. Hopkins
Extreme Thermal Materials
U. of Virginia · 2025–Present

Dr. Peter Hosemann
Materials Joining & Structural Integrity
UC Berkeley · 2025–Present

Dr. Travis W. Knight
Advanced Nuclear Fuels & Systems
U. of South Carolina · 2025–Present

Dr. Philippe Lebrun
Cryogenics & Magnet Cooling
CERN · 2025–Present

Dr. Nitendra Singh
Nuclear Safety & Fuel Cycle
ITER · 2025–Present

Dr. Guido Van Oost
Magnetic Confinement & Fusion Systems
Ghent University · 2025–Present

Dr. Gary S. Was
Radiation Materials & Structural Integrity
U. of Michigan · 2025–Present

Dr. Ray Sedwick
Direct Energy Conversion
U. of Maryland · 2025

OPERATIONS

Michael Laughlin
Chief Operating Officer
2022–Present

Martin Owens
Chief Strategy Officer
LANL / GE Hitachi · 2022–Present

MG (Ret.) Paul Pardew
Chief Contracting Officer
Army Contracting Command · 2022–Present

David Beck
Fusion Commercialization
U.S. Space Force · 2024–Present

Sushma Bhatia
Environmental & Legislative
Google · 2022–Present

Michael De Frenza
Technology Licensing
2023–Present

MG (Ret.) Robin L. Fontes
Cybersecurity & Defense
Army Cyber Command · 2022–Present

Vijay Gehani
Supply Chain & Components
INOX India · 2024–Present

Jon Michel Greenwood
IT & AI Infrastructure
Live Nation · 2023–Present

Brian C. O'Neill
National Security
CIA / ODNI · 2022–Present

Gen. (Ret.) Gustave F. Perna
DoD Liaison
Operation Warp Speed · 2022–2023

Andrea Romero
Marketing Lead
2022–Present

Legal counsel is retained; those roles are held on the internal roster and are not listed here.

SOURCES

References

1 P I Ford, *Kronos Physics De-Risking Register*, Kronos Fusion Energy 2026 series, doi:10.5281/zenodo.22133057.

2 V S Mukhovatov and V D Shafranov, "Plasma equilibrium in a tokamak," *Nucl. Fusion* **11**, 605 (1971).

3 E A Lazarus, J B Lister and G H Neilson, "Control of the vertical instability in tokamaks," *Nucl. Fusion* **30**, 111 (1990), doi:10.1088/0029-5515/30/1/010.

4 A Portone, "The stability margin of elongated plasmas," *Nucl. Fusion* **45**, 926 (2005), doi:10.1088/0029-5515/45/8/021.

5 D A Humphreys *et al.*, "Experimental vertical stability studies for ITER performance and design guidance," *Nucl. Fusion* **49**, 115003 (2009), doi:10.1088/0029-5515/49/11/115003.

6 R Albanese and F Villone, "The linearized CREATE-L plasma response model for the control of current, position and shape in tokamaks," *Nucl. Fusion* **38**, 723 (1998), doi:10.1088/0029-5515/38/5/307.

7 R Albanese, R Ambrosino and M Mattei, "CREATE-NL+: a robust control-oriented free boundary dynamic plasma equilibrium solver," *Fusion Eng. Des.* **96–97**, 664 (2015), doi:10.1016/j.fusengdes.2015.06.162.

8 M Ariola and A Pironti, *Magnetic Control of Tokamak Plasmas*, 2nd ed., Springer (2016).

9 G Ambrosino and R Pironti, "Magnetic control of plasma current, position, and shape in tokamaks," *IEEE Control Syst. Mag.* **25**(5), 76 (2005).

10 G De Tommasi, "Plasma magnetic control in tokamak devices," *J. Fusion Energy* **38**, 406 (2019).

11 M L Walker and D A Humphreys, "Valid coordinate systems for linearized plasma shape response models in tokamaks," *Fusion Sci. Technol.* **50**, 473 (2006).

12 J P Freidberg, *Ideal Magnetohydrodynamics*, Plenum Press, New York (1987).

13 J Wesson, *Tokamaks*, 4th ed., Oxford University Press (2011).

14 S C Jardin, *Computational Methods in Plasma Physics*, CRC Press, Boca Raton (2010).

15 L L Lao *et al.*, "Reconstruction of current profile parameters and plasma shapes in tokamaks," *Nucl. Fusion* **25**, 1611 (1985).

16 B Dudson *et al.*, *FreeGS: free-boundary Grad–Shafranov equilibrium solver*, (2020), doi:10.5281/zenodo.3745669.

17 C R Sovinec *et al.*, "Nonlinear magnetohydrodynamics simulation using high-order finite elements," *J. Comput. Phys.* **195**, 355 (2004), doi:10.1016/j.jcp.2003.10.004.

18 T C Hender *et al.*, "Progress in the ITER Physics Basis, Chapter 3: MHD stability, operational limits and disruptions," *Nucl. Fusion* **47**, S128 (2007).

19 ITER Physics Expert Group on Disruptions, Plasma Control, and MHD, "ITER Physics Basis, Chapter 3: MHD stability, operational limits and disruptions," *Nucl. Fusion* **39**, 2251 (1999).

20 R S Granetz *et al.*, "Disruptions and halo currents in Alcator C-Mod," *Nucl. Fusion* **36**, 545 (1996).

21 N W Eidietis *et al.*, "The ITPA disruption database," *Nucl. Fusion* **55**, 063030 (2015).

22 M Lehnen *et al.*, "Disruptions in ITER and strategies for their control and mitigation," *J. Nucl. Mater.* **463**, 39 (2015).

23 E M Hollmann *et al.*, "Status of research toward the ITER disruption mitigation system," *Phys. Plasmas* **22**, 021802 (2015).

24 D A Gates *et al.*, "Plasma vertical position control in the National Spherical Torus Experiment," *Nucl. Fusion* **46**, 17 (2006).

25 S P Gerhardt *et al.*, "Detection of disruptions in the high-β spherical torus NSTX," *Nucl. Fusion* **53**, 063021 (2013).

26 J E Menard *et al.*, "Fusion nuclear science facilities and pilot plants based on the spherical tokamak," *Nucl. Fusion* **56**, 106023 (2016).

27 A Sykes *et al.*, "First results from MAST," *Nucl. Fusion* **41**, 1423 (2001).

28 D J Battaglia *et al.*, "Implications of vertical stability control on the SPARC tokamak," arXiv:2401.09613 (2024).

29 A J Creely *et al.*, "Overview of the SPARC tokamak," *J. Plasma Phys.* **86**, 865860502 (2020).

COLOPHON

How this document was made

The Kronos Fleet — Combined Editorial, 2026 is set in **Fraunces** (display), **Gelasio** (text), and **IBM Plex Mono** (data & equations), carried forward from the Kronos editorial design system.

The figures are rendered at 300 dpi from the deposited generator scripts; the document is composed as a single self-contained file with embedded fonts and imagery, paginated to US Letter, and rendered to PDF through a headless Chromium engine in matched light and dark editions.

Every headline quantity carries an evidence class; withdrawn and restated values are marked as such. Nothing herein is frozen beyond the founder-approved Tier-A set.

Explore it live — turn the interactive 3-D model, run the deposited solvers in the physics validator, and watch the companion film series.

LEGAL NOTICE

Notice, status, and distribution

Conceptual design & simulation study. This document reports a conceptual design and simulation study. It is not a construction commitment, a safety-analysis report, a regulatory filing, or an offer of securities. Forward-looking statements — schedules, costs, market sizes, and performance — are estimates subject to the limitations set out in the Simulations part and may change.

Numbers and their classes. Quantities are reported with evidence classes and case labels; modelled, assumed, and requirement-class values are identified as such and are not to be quoted without their labels.

Public edition. This edition carries the physics and design only; all financial, funding, and defense-commercial content has been removed for public distribution. The scientific text corresponds to the arXiv and journal submissions.

THE 2026 KRONOS SERIES

One programme, many papers

This editorial is one paper in the Kronos 2026 series — a real fusion company's complete, reproducible physics record for a spherical-tokamak breeder and its low-neutron D–^{3}He tandem-mirror burners. Every headline number is a frozen anchor in the Physics De-Risking Register.

Explore the whole programme: the De-Risking Register, the interactive 3-D model, and the physics validator.

KRONOS FUSION ENERGY

Vertical Stability at High Elongation: Displacement Growth Rates, Control-Coil Authority, and VDE Avoidance for a Compact Spherical-Tokamak Breeder

A real fusion company building real machines. Explore the science, live.

Zenodo · doi:10.5281/zenodo.22645834

Read on kronosfusionenergy.com

The Physics De-Risking Register